Available online at www.sciencedirect.com
ScienceDirect
Cement and Concrete Research 36 (2006) 1768–1776
Cement and Concrete Research

Isothermal moisture properties of Clayey Cellular Concretes elaborated from clayey waste, cement and aluminium powder

M.S. Goual [a], A. Bali [b], F. de Barquin [c], R.M. Dheilly [d], M. Quéneudec [d,*]

[a] *Laboratoire de Génie Civil, Université de Laghouat, B.P 37G, (03000) Laghouat, Algeria*
[b] *Laboratoire de construction et environnement, Ecole Nationale Polytechnique d'Alger, El-harrach, Algeria*
[c] *C.S.T.C, Division Matériaux, 21 Avenue Pierre Holoffe, 1342 Limelette, Belgium*
[d] *Laboratoire des Technologies Innovantes, Université de Picardie Jules Verne, IUT d'Amiens, Département de Génie Civil, Avenue des Facultés, Le Bailly, 80025 Amiens Cedex 01, France*

Received 9 December 2003; accepted 9 December 2005

Abstract

This paper describes a study undertaken to examine the moisture behaviour, in either the vapour or liquid phase of a series of six Clayey Cellular Concrete (CCC) mixes featuring different porosities. These mixes have been obtained by expanding a clay–cement paste through adding a small quantity of aluminium powder during mixing. The material porosity analysis performed using mercury intrusion porosimetry shows that two classes of porosity in the materials derived may be distinguished: microporosity within the clay–cement matrix and macroporosity in the form of gaseous cells dispersed within the matrix, resulting from the chemical reaction between aluminium powder and lime freed at the time of cement hydration. Macroporosity would thus constitute the parameter that differentiates all CCC mixes. Another purpose of the present work is to display how the moisture properties of homogeneous porous materials are expected to change as the macroporosity rate changes. On the basis of experimental results, it will be demonstrated that macroporous cells serve to diminish both the adsorption capacity and sorptivity of CCC; however hydraulic diffusivity in the capillary process increases as a function of macroporosity.

Keywords: Lightweight concrete; Mercury porosimetry; Pore size distribution; Transport properties; Mortar

1. Introduction

The durability of building materials is very sensitive to humidity; both high and low moisture contents as well as abrupt content changes, may cause problems, damage the materials and reduce their mechanical and thermal performances. An improved understanding of moisture transport can therefore serve to limit or prevent damage in building materials, and hence in components of the building envelope. These phenomena are of great interest to physicists and engineers working in the areas of heat and mass transfer [1] and building materials [2].

As new data on sorption isotherms, sorptivity and hydraulic diffusivity have become available; it is now possible to examine how the measured values of these moisture properties vary from one material to the next in response to differences in both material composition and porous structure. When modelling moisture transport, the concept of unsaturated flow is increasingly adopted [3–8] and several research efforts have been pursued in order to predict moisture transport coefficients through establishing relationships between moisture properties and structure porosity [9–15].

In the aim of enhancing the reuse of clayey by-products, the notion of their transformation into building materials and especially thermal insulation building materials becomes very attractive not just from economic perspective but from an environmental one as well. Such objectives have led to developing Clayey Cellular Concretes (CCC) by means of expanding a clay–cement paste through adding a small quantity of aluminium powder during mixing. These concretes are composed of clayey type kaolinites stabilised with a small

* Corresponding author. Tel./fax: +33 3 22 53 40 16.
E-mail address: Michele.tkint@iut.u-picardie.fr (M. Quéneudec).

0008-8846/$ - see front matter © 2006 Elsevier Ltd. All rights reserved.
doi:10.1016/j.cemconres.2005.12.017

quantity of cement. In general, cellular concretes are manufactured using an autoclaving process along the lines of Autoclaved Aerated Concrete AAC, yet this process remains very costly due to the need for an autoclave and the high energy consumption involved. Clayey Cellular Concretes however are produced at room temperature and without any autoclaving [16]. In order to predict the durability of the materials generated, a study of their moisture behaviour thus proves essential. In this study, experimental results on moisture properties of CCC determined at isothermal conditions are presented, with consideration given for either the vapour or liquid humidity states. A series of six mixes with varying porosities has been elaborated and examined herein. Mercury intrusion porosimetry analysis shows that CCC materials exhibit dual porosity: a microporosity localised essentially in the clay–cement matrix and a macroporosity dispersed within the matrix in form of gaseous cells, as produced by chemical reaction with the aluminium powder. Macroporosity thus constitutes the structural variable parameter that differentiates all CCC mixes. Another purpose herein is to show how moisture properties of the materials derived are expected to change as the macroporosity rate changes.

2. Theoretical aspects of water absorption

Given the assumption that the interaction of vapour, liquid and solid phases may be neglected, at least two distinct techniques for retaining water within porous building materials are available. First, as the relative humidity of the surrounding air gradually increases, the porous material once takes up water again by means of adsorption and capillary condensation. Second, if the surface of the structural element lies in contact with liquid water, the material absorbs water quickly by capillary suction.

During the adsorption process water vapour molecules within the surrounding environment are attracted toward the material interface due to Van Der Waals' Forces. As this process unfolds, various water-fixation steps can be distinguished [17–19]. The first is monomolecular adsorption, in which a single water molecule layer covers the pore surfaces; this step can be observed at low relative humidity levels (less than 0.10). The second step is characterised by the fixation of multilayer water molecules on pore surfaces when relative humidity is between 0 and 0.40. Lastly, and at high relative humidity levels (more than 0.40), liquid bridges can appear in between the pore wall, characteristic of the capillary condensation phase. The evolution curve of water content in the porous material as a function of relative humidity at a given temperature is known as the isotherm adsorption curve. For this particular case, a relationship between surface tension and vapour pressure exerted at the vapour–liquid interface known as Kelvin–Laplace equation [20] is given below.

$$\phi = \frac{P_v}{P_{vs}} = \exp\left(-\frac{2\sigma M}{\rho_w RTr}\right) \tag{1}$$

where ϕ is the relative humidity, σ the air/water surface tension (≈0.0728 N/m at 20 °C), ρ_w the volumetric mass of water (≈998.3 kg/m^3 at 20 °C), M the molar mass of water (≈18.10^{-3} kg/mol), T the temperature (K), R the perfect gas constant (=8.3143 J/mol/K) and r the pore radius.

From Eq. (1) a pore radius size limit that serves to distinguish hygroscopic pores from capillary pores may be determined. At ambient temperature T=20 °C (293 K) and for $\phi \approx 0.989$ corresponding to the critical water content, this limit is about 0.1 μm. Such a finding allows us to differentiate hygroscopic materials from capillary materials. For the hygroscopic materials, the quantity of water absorbed is relatively high with respect to the material saturation threshold; the pore radius for such a class is less than 0.1 μm. For capillary materials, the quantity of adsorbed water, as relative humidity reaches 98.9%, is very low in comparison with the total volume of accessible pores. The saturation of such material may only be achieved by capillary suction when the material is placed in contact with liquid water. In this case the capillary pressure P_c thereby created tends to attract water inside the porous network. For a cylindrical pore model, capillary pressure is given by the Laplace law expressed as follow:

$$P_c = \frac{2\sigma \cdot \cos\beta}{r} \quad [\text{Pa}] \tag{2}$$

where σ and r are as defined above; β is the contact angle defining liquid wettability on the given solid surface (water is considered herein as a perfectly wetting fluid, then, β=0).

Capillary suction ψ is the capillary pressure expressed in water height column, thus:

$$\psi = -\frac{P_c}{\rho_w g} \quad [\text{m}] \tag{3}$$

where g is the gravity acceleration (≈9.81 m/s^2).

When neglecting gravitational effect, the isothermal moisture transport in porous materials is generally described using Philip and De Vries simplified model [21] given as follow:

$$\frac{\partial \theta}{\partial t} = \text{div}(D_\theta \nabla \theta) \tag{4}$$

θ, is the volumetric water content; D_θ the hydraulic diffusivity (m^2/s) and t, the time (s).

This expression is subject to the appropriate initial and boundary conditions. For the one-dimensional case of water absorption through the end face of a long bar for example, we have:

$$\frac{\partial \theta}{\partial t} = \frac{\partial}{\partial x}\left(D_\theta \frac{\partial \theta}{\partial x}\right) \tag{5}$$

$$\theta = \theta_s \text{ at } x = 0, t \geq 0$$

$$\theta = \theta_0 \text{ for } x \rangle 0, \; t = 0.$$

Using the Boltzmann transform $b=x\cdot t^{-0.5}$ Eq. (5) reduces to an ordinary differential equation:

$$-\frac{b}{2}\frac{\mathrm{d}\theta}{\mathrm{d}b}=\frac{\mathrm{d}}{\mathrm{d}b}\left(D_\theta\frac{\mathrm{d}\theta}{\mathrm{d}b}\right) \tag{6}$$

With $\theta=\theta_s$ at $b=0$; and $\theta=\theta_0$ as $b\to\infty$,

Hydraulic diffusivity D_θ at the volumetric water content θ is then obtained from integrating Eq. (6), hence:

$$D_\theta=-\frac{1}{2}\frac{\mathrm{d}b}{\mathrm{d}\theta}\int_{\theta_0}^{\theta} b\cdot\mathrm{d}\theta \tag{7}$$

From the solution θ (b), the total water content i (t) per unit area may be calculated as

$$i(t)=t^{1/2}\int_{\theta_0}^{\theta_s} b\cdot\mathrm{d}\theta=S_w t^{1/2} \tag{8}$$

This relation serves to define material sorptivity S_w of the material at both the initial and final states $\theta=\theta_0$, θ_s. Moreover, it represents the rate of water penetration, with high-quality concrete being indicated by low water sorptivity values. See Refs. [3,5,7,8] for more details.

Furthermore, the isotherm sorption curves, sorptivity and hydraulic diffusivity mentioned above constitute the target moisture properties.

3. Materials and experimental set up

3.1. Materials

The Clayey Cellular Concretes produced herein are composed of clayey fines (containing almost exclusively kaolinites) stabilised with a Portland cement (CPA CEM I 52.5). The composition in terms of weight percentage of dry clay–cement materials for CCC samples amounts to 75% clay and 25% cement. The percentage of mixing water which has been optimised in order to satisfy both the workability criterion and the RILEM recommendations [22], represent 65% of the dry clay–cement weight. Six compositions of CCC have been produced with aluminium powder percentages varying from 0% to 1% by increments of 0.2%. A more detailed description of the materials and sample preparation is provided in Refs. [4] and [16]. Table 1, gives the thermal and mechanical characteristics of all CCC mixes measured after 28 days of conservation at 20 °C and 90% relative humidity.

Table 1
Physical, mechanical and thermal characteristics of all CCC mixtures

CCC mixture	Relative mass percentage of aluminium powder Al/(Clay+Cement)	Bulk density (kg/m^3)	28-day compressive strength (MPa)	Dry thermal conductivity (W/m/K)
A (matrix)	0.00	1038	3.85	0.281
B	0.20	962	3.15	0.264
C	0.40	953	2.40	0.235
D	0.60	903	1.85	0.223
E	0.80	876	1.20	0.216
F	1.00	843	0.95	0.201

3.2. Experimental setup

3.2.1. Porosity identification

Among the set of parameters representing pore structure, total porosity (pore volume fraction), specific surface area and pore size distribution prove to be especially important. Three methods have been applied to determine the density and porosity of the materials developed: mercury intrusion porosimetry, vacuum saturation and pycnometry.

Mercury intrusion porosimetry was carried out by means of an Autopore III 9420, manufactured by Micrometrics Corp. The characteristics of the mercury used in these experiments are $\beta=142°$, $\sigma=0.485$ N/m and $d_0=13.53$, respectively, for contact angle, surface tension and density. Further details on the mercury porosimetry method are provided in Refs. [11,23,24].

The principle behind the method consists of immersing a representative sample volume of about $10\times10\times20$ mm previously purged of all constituent air in mercury at the lowest pressure generated by the apparatus. In this manner, the sample volume V may be determined. The mercury pressure P_{Hg} is then gradually increased; for each pressure level until reaching equilibrium, the penetrated volume V_{Hg} is measured from the beginning of the test onward. When the maximum pressure has been reached (about 400 MPa), both the accessible pore volume and principal intrusion curve $V_{Hg}=f(P_{Hg})$ can also be determined.

By substituting mercury characteristics in Eq. (2), pore diameters $D=2r$ may be expressed as function of mercury pressures P_{Hg} as follow:

$$D(\mu\mathrm{m})=\frac{15.287}{P_{Hg}[\mathrm{bars}]}. \tag{9}$$

Using Eq. (9), the primary intrusion curve can be expressed as a function of pore diameters $V_{Hg}=f(D)$, and is known as the pore size distribution curve.

Given that mercury porosimetry may not be straightforward to implement should the applied pressure not fill all of the pores, since micropores are not accessible by means of mercury intrusion; both the vacuum saturation and pycnometry methods have been used herein in order to estimate the rate of porosity explored by mercury porosimetry. The experimental set-up complies with all pertinent recommendations [25,26].

3.2.2. Sorption measurements

The sorption measurements were conducted using the installation shown in Fig. 1. Samples of about $20\times20\times10$ mm^3 in size were dried and placed in an atmospheric chamber. The temperature controlled chamber serves to maintain the entire thermostatic chamber as well as the saturation system at the desired temperature. This configuration prevented the

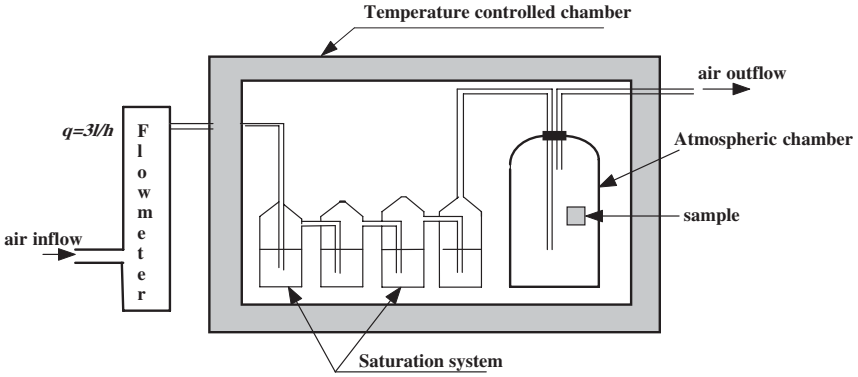

Fig. 1. Experimental apparatus for isothermal sorption measurement.

appearance of any cold points that could modify the desired H_2O pressure.

The atmosphere within the test chamber was maintained at the desired level by means of circulating air from the saturation system. The amount of air introduced into the apparatus was metered in order to ensure that experimental conditions were held constant. The desired relative humidity ϕ was obtained through application of a water and sulphuric acid (17.82 M) mix. Concentrations were chosen on the basis of the relationship between relative humidity and density of sulphuric acid solutions (see Table 2) [27].

During testing, each sample was monitored using gravimetric analysis, i.e. weighing every day until the weight has stabilised. For each composition category, variations in sample mass as a function of time reach a plateau in approximately 12 days.

3.2.3. Capillary imbibition test

According to test protocol, the studied sample (40×40×160 mm) which was initially dried at 70 °C until reaching constant mass, is sealed laterally with a plastic film to ensure a one dimensional flow. One of the unsealed surfaces is placed in contact with liquid water (20 °C) at a depth of approximately 3 mm, as shown in Fig. 2, with the water level in the pan being held constant throughout the experiment.

Table 2
Relative humidity, vapour pressure and sulphuric acid solution density rapport

H_2SO_4 density	Relative humidity ϕ (%)	Vapour pressure P_v (10^{-3} bars)
1.00	100.0	17.4
1.05	97.5	17.0
1.10	93.9	16.3
1.15	88.8	15.4
1.20	80.5	14.0
1.25	70.4	12.2
1.30	58.3	10.1
1.35	47.2	8.3
1.40	37.1	6.5
1.50	18.8	3.3
1.60	8.5	1.5
1.70	3.2	0.6

Total water content $i(t)$ per unit surface area is then measured by weighing the sample at regular intervals using a 0.01-g precision scale. The following formula is then applied:

$$i(t) = \frac{M(t) - M(0)}{A\rho_w} \quad \left[\mathrm{m}^3/\mathrm{m}^2\right] \tag{10}$$

where $M(t)$ is the sample mass measured after t time spent in contact with water; $M(0)$ is the initial dried mass of the sample and A is the section area in contact with water ($A = 40 \times 40$ mm^2).

The plot of cumulative water absorption versus the square root of time enables determining the sorptivity coefficient.

The hydraulic diffusivity or capillary transport coefficient of the derived materials has been identified by measuring moisture profiles at various heights using a gravimetric technique [4]. Application of the Boltzmann transformation allows combining the various measured moisture profiles into a single profile that serves to determine hydraulic diffusivity by using Eq. (7).

4. Experimental results and discussions

4.1. Characterisation of porous structure

The total porosity measurements obtained from the various techniques explained above have been listed in Table 3, which reveals the strong similarity among results. This finding led us to suppose that nearly all porosity values for the entire set of

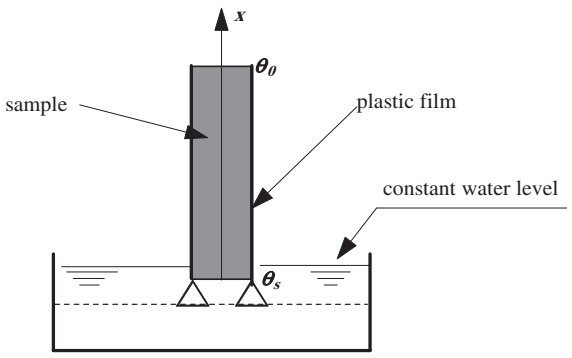

Fig. 2. A one dimensional capillary imbibitions test.

Table 3
Results of total porosity obtained by various methods

CCC mixture	Aluminium percentage	Pycnometry	Vacuum saturation	Mercury porosimetry	Average values
A (matrix)	0.00	0.577	0.581	0.579	0.579
B	0.20	0.595	0.596	0.591	0.594
C	0.40	0.618	0.619	0.620	0.619
D	0.60	0.641	0.634	0.630	0.635
E	0.80	0.678	0.649	0.662	0.663
F	1.00	0.704	0.651	0.670	0.675

mixes had been explored. The normalised pore size distribution curves using mercury porosimetry intrusion are presented in Fig. 3.

For the purpose of this exercise it has been assumed that cells created within the material by adding aluminium powder cannot modify in any way the microporous matrix structure. Fig. 3 indicates that adding aluminium powder subdivides total porosity into two distinct classes. Consequently, the matrix (composition A) is composed exclusively of pores with diameters less than 1 μm, this class is referred to as micropores. The other class of pores ($D>1$ μm) is referred to as macropores and features a porosity that stems from the chemical reaction between aluminium powder and clay–cement paste. This reaction can be explained as follow [28]:Initially, the lime freed at the time of cement hydration dissolves in aqueous phase as:

$$Ca(OH)_2 \rightarrow Ca^{2+} + 2(OH)^-$$

Next, during a second stage:

$$2Al + 2(OH)^- + 4H_2O \rightarrow 2AlO(OH)_2^- + 3H_2\nearrow$$

This reaction clarifies that the expansion phenomenon is caused by the release of the gaseous hydrogen that provides the material with its cellular structure.

It should be noted that the pH of the medium is about 12.5 [29] and that the calcium hydroxide freed by cement hydration will attack the surface of clay particles under highly basic conditions; such a condition induces the dissolution of silicium and aluminium oxides making with Ca^{2+} an insoluble product cementing the clay particles. This reaction has been studied by many authors such as Za-Chiem Moh [30] who showed that the major products generated are hydrated calcium silicates and aluminates. Some studies have been conducted [31,32] on the specific factors influencing the kaolinite–cement reaction. Mitchell and El Jack [33], studying the reaction kinetics for a kaolinite/cement ratio close to the value used herein, demonstrated in particular that a clay particle interconnection appears and after 32 weeks it becomes impossible to distinguish the cement phase from the kaolinite phase. The kaolinite–cement reaction is slow compared with cement hydration. In this work, the samples have been aged 28 days. Consequently, the kaolinite–cement reaction is not very well advanced.

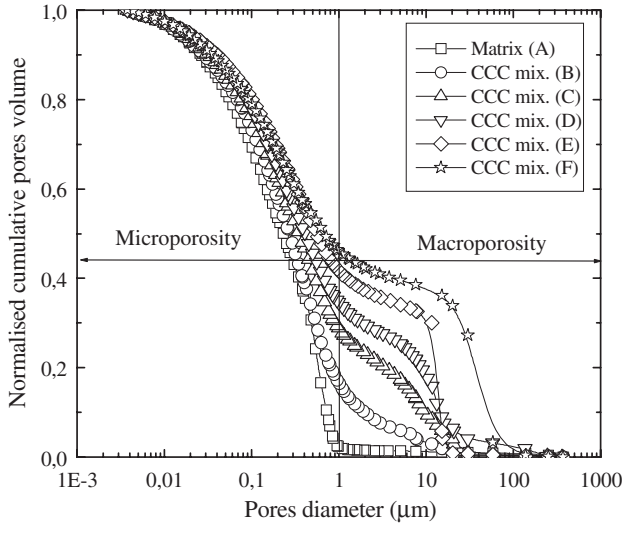

Fig. 3. Normalised pore size distribution curves for all CCC mixtures.

As regards mercury porosimetry results (Fig. 3), both the microporosity and macroporosity rates in all CCC compositions have been reported in Table 4.

4.2. Moisture properties

4.2.1. Sorption isotherms

Fig. 4 shows all the sorption isotherm curves. Experimental results were derived as the mean of three independent measurements conducted on three samples of each CCC compositions. The relationship between mass water content (ω) and relative humidity (ϕ), denoted $\omega(\phi)$, is a non-linear increasing function. The curves were smoothed using the Hillerborg model [18] developed on the basis of BET theory [34]. This model has already been validated in the case of autoclaved aerated concrete [6].

Experimental results reveal that a small amount of water is absorbed back into Clayey Cellular Concretes whenever the relative atmospheric humidity is less than 70%. Beyond this threshold, the increase in water content proves to be very significant. We can also note that the critical water content (ω_c) reached at approximately 98.9% decreases as macroporosity increases as shown in Fig. 6. Its value varies from 0.07 kg/kg for the matrix (A) to 0.052 kg/kg for the composition (F), a range that corresponds respectively to 12.55% and 6.50% of the material saturation threshold. This drop in maximum water

Table 4
Microporosity, macroporosity and specific surface area of pores for all CCC mixtures

CCC mixture	Total porosity (ε_0)	Microporosity ($\varepsilon_{\mu p}$)	Macroporosity (ε_{mp})	BET specific surface area of pores (m^2/g)
Matrix (A)	0.579	0.579	0.000	14.391
B	0.594	0.497	0.097	14.113
C	0.619	0.440	0.179	10.774
D	0.635	0.417	0.218	3.983
E	0.663	0.388	0.275	3.109
F	0.675	0.366	0.309	1.847

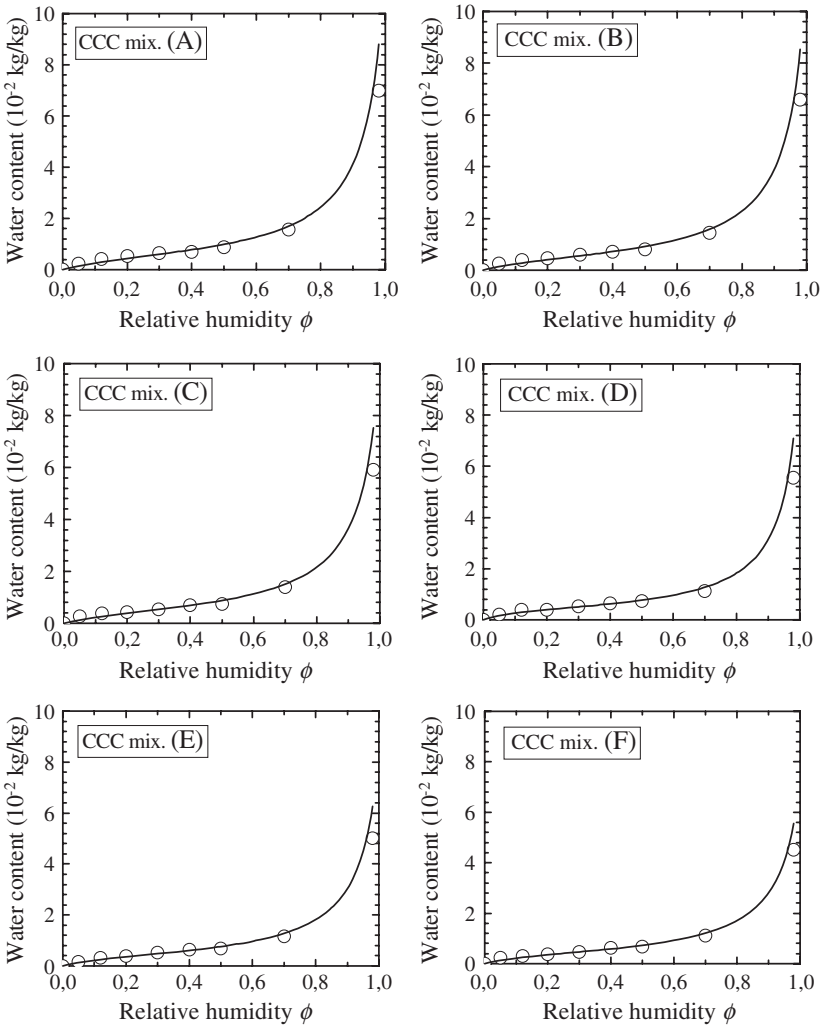

Fig. 4. Sorption isotherm curves of various Clayey Cellular Concrete mixtures.

absorption by means of physical adsorption is essentially due to the fact that capillary condensation in macropores does not start until the relative humidity values lie very close to 100%.

Furthermore, the small quantity of water absorbed by physical adsorption, in comparison with the quantity at saturation, proves that CCC does not exhibit hygroscopic behaviour, as opposed to similar materials such as Autoclaved Aerated Concretes (AAC) [35]. The low values of pore specific surface area (see Table 4) determined using the BET model reflect the presence of a small proportion of hygroscopic pores. The decrease in pore specific surface area as a function of macroporosity rate allows us to conclude that the presence of macroporous cells within building materials attenuates the capacity of materials to adsorb water in the surrounding atmosphere. In our particular case, macroporosity reduces maximum water adsorption by a factor of: $1-0.377\varepsilon_{mp}-1.464\varepsilon_{mp}^2$ with a correlation coefficient of 0.9988, as shown in Fig. 5. ε_{mp} is macroporosity.

4.2.2. Capillary imbibitions properties

The temporal evolution of total water content $i(t)$ in the sample per unit area (suction curve) was measured by precise weighing. In Fig. 6, this reduced-scale figure displays an example of suction curves as a function of the square root of time for (A) and (F) mixes, representing the lower and higher CCC porosity levels. This figure indicates that, before mass stabilisation, all suction curves are linear functions of the square

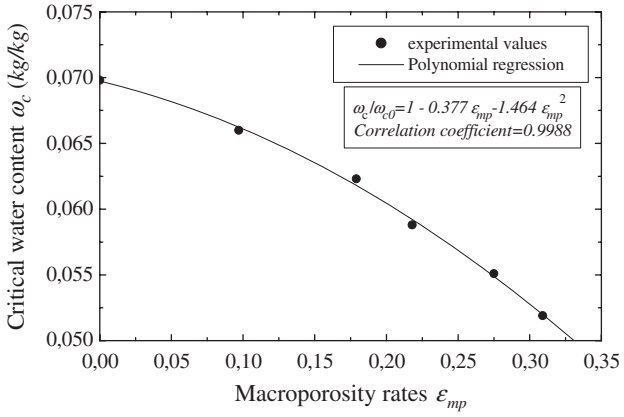

Fig. 5. Critical water content as function of macroporosity rates.

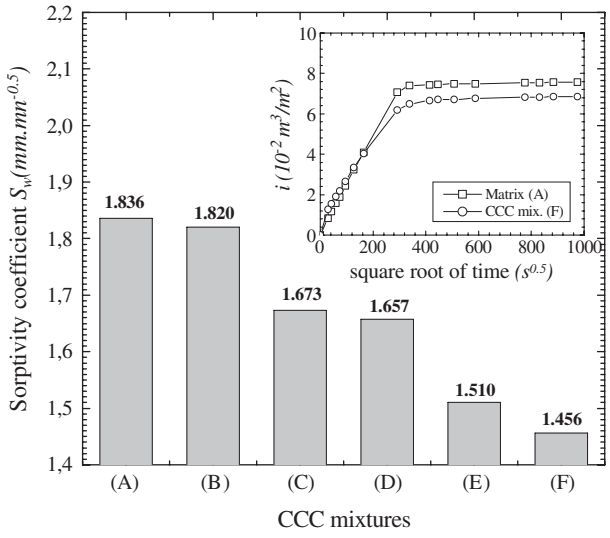

Fig. 6. Sorptivity coefficients for all CCC mixtures.

root of time as given by Eq. (8) with a small intercept at $t=0$; in this case, an additional term i_0 would need to be included in the equation, hence:

$$i(t) = S_w \cdot t^{1/2} + i_0 \qquad (11)$$

According to Hall and Kam-Ming TSE [36], the quantity i_0 results from the rapid filling of open pores on the side faces of the test specimen.

Fig. 6 also presents experimental values of sorptivity coefficients for all CCC compositions. This figure shows that sorptivity decreases as a function of macroporosity. It should be pointed out that the total water content values measured at equilibrium are approximately $\theta=0.510$ for matrix (A), whereas total porosity is $\varepsilon_0=0.579$; this water content amount drops to just $\theta=0.386$ for mix (F) while total porosity stands at $\varepsilon_0=0.675$. These results have led us to consider that all micropores in the matrix are basically saturated with water; in contrast, only the microporous portion of composition (F) $\varepsilon_{\mu p}=0.366\approx\theta$ is completely saturated. Consequently, the macropores, due to hydrogen gas release, are not involved in the capillary imbibition process. Their role therefore is to create tortuous paths that elongate water flow routes. This contribution provides a rationale for the decrease in sorptivity coefficient as a function of macroporosity. In normalised sorptivity terms, the following formula is established between sorptivity and rate of macroporosity.

$$\frac{S_w}{S_{w0}} = 1.00 - 0.056\varepsilon_{mp} - 2.087\varepsilon_{mp}^2 \qquad (R = 0.9913) \qquad (12)$$

where S_{w0} is the sorptivity coefficient of the matrix (mixture A).

The moisture profiles and hydraulic diffusivities measured during the absorption process have been given in a previous study (see Ref. [4]). Hydraulic diffusivity D_θ results, which are known as the capillary transport coefficient of matrix (A), along with the (C) and (F) Clayey Cellular Concrete compositions have been replicated in Fig. 7. This figure shows that hydraulic diffusivity increases with macroporosity and can be explained by the fact that capillary invasion tends to arise mainly through homogeneous small-radius paths (micropores); at a certain stage, this phenomenon leads to excluding those macropores in which a gas will definitely be occluded. The surface area provided for diffusion phenomena therefore becomes progressively reduced as macroporosity increases, which incites an increase in the diffusion coefficient. This same phenomenon has been observed in wood-cementitious composites [10] and this moisture transfer has been compared to that appearing with autoclaved aerated concrete (AAC). The notably weaker capillary transport coefficient may be connected to the production process. During AAC curing which takes place under high temperature and high pressure in saturated steam, a portion of siliceous sand chemically reacts with lime and lead to a micro-crystalline structure that, to a large extent, is composed of crystalline tobermorite, which proves more stable than products formed in normally cured concretes. A comparison [14] of the capillary behaviour of AAC and unautoclaved aerated concrete indicates their behavioural differences and provides one possible explanation for such differences in the formation of cracks due to drying shrinkage.

5. Conclusion

In this paper, an experimental investigation on the isothermal moisture properties of Clayey Cellular Concretes at various porosities has been conducted. The purpose herein has also been to demonstrate how macroporous structures can affect CCC moisture properties. Based on the results of this investigation, the following conclusions may be drawn:

1. Porosity identification, as performed by Mercury Intrusion Porosimetry (MIP), has revealed the existence of two distinct pores classes: micropores in the matrix and macropores or gaseous cells, resulting from the addition of aluminium powder at the time of mixing, dispersed within the matrix. The pore diameter threshold that distinguishes these two porosity classes has been estimated at 1 μm.

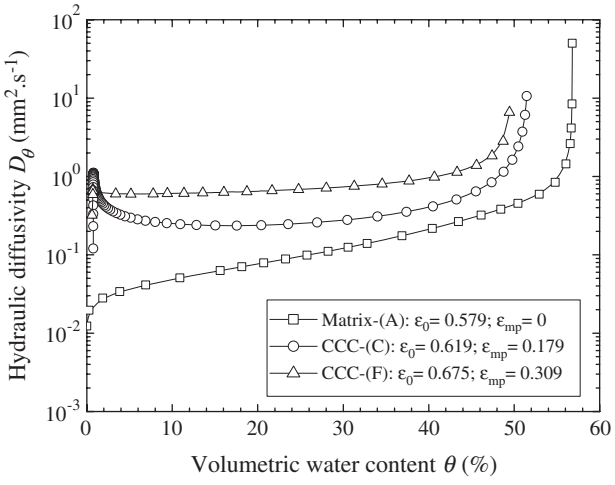

Fig. 7. Hydraulic diffusivity as function of volumetric water content for (A), (C) and (F) CCC mixtures.

2. The comparison between total porosity values measured using the MIP method and those obtained by either the vacuum saturation or pycnometry method indicates a high level of similarity, which leads us to suppose that nearly all porosity values for the entire set of CCC mixes have been explored.
3. The isotherm adsorption curves reveals that all CCC mixes are non-hygroscopic materials. The maximum water content ω_c adsorbed by all compositions at a relative humidity of 98.9% is thus significantly less than the material saturation threshold. It has also been shown that macroporosity reduces the critical water content by a factor of $(1-0.377\varepsilon_{mp}-1.464\varepsilon_{mp}^2)$ approximately. Moreover, it has been found that Hillerborg's model used for smoothing sorption isotherms accurately reconstruct experimental results of adsorption tests.
4. In the capillary imbibitions testing series, it was confirmed that all suction curves for CCC mixes are fully described by the well-known $\sqrt{t}$−law. New data on sorptivity coefficients of CCC mixes with macroporosity rates ranging from 0% to 31% indicate that macroporosity serves to reduce sorptivity by a factor of $(1-0.056\varepsilon_{mp}-2.087\varepsilon_{mp}^2)$ approximately.
5. Hydraulic diffusivity D_θ results, as a function of volumetric water contain for three different CCC mixes with a macroporosity rate of roughly 0%, 18% and 31% demonstrate that prior to total saturation, hydraulic diffusivity in the capillary process increases slowly as a function of water content. This trend slows when macroporosity increases and becomes faster as water content reaches the material saturation thresholds. It has also been shown that hydraulic diffusivity increases as a function of the macroporosity rate.
6. Lastly, when used as an interior building material, CCC can provide satisfactory thermal and moisture comfort due to its non-hygroscopic behaviour. When CCC is exposed to outside air however, protective measures against liquid water infiltration must be taken into consideration due to the material's ability to absorb water by means of capillary suction.

References

[1] J.B. Chaddock, B. Todorovic (Eds.), Heat and Mass Transfer in Building Materials and Structures, 21st Symp. of the Int. Center for Heat and Mass Transfer, Hemisphere, New York, 1990.

[2] R.K. Dhir, J.W. Green, Pr. Int. Conf. on the Protection of Concrete held at the University of University of Dundee, Scotland UK, in: R.K. Dhir, J.W. Green (Eds.), E & FN Spon, London, 1990.

[3] C. Hall, W.D. Hoff, William: Water Transport in Brick, Stone and Concrete, E & FN Spon, London, 2002.

[4] M.S. Goual, F. de Barquin, M.L. Benmalek, A. Bali, M. Quéneudec, Estimation of the capillary transport coefficient of clayey aerted concrete using a gravimetric technique, Cement and Concrete Research 30 (2000) 1559–1563.

[5] M.K. Humaran, Moisture diffusivity of building materials from water absorption measurement, Thermal Envelop and Building Science 22 (1999) 349–355.

[6] D. Quénard, Adsorption et transfert d'humidité dans les matériaux hygroscopiques: Approche de type percolation et expérimentation, Thèse de Doctorat, INP Toulouse (France), 1989.

[7] J. Gummerson, C. Hall, W.D. Hoff, Water transport in porous building materials-II, hydraulic suction and sorptivity of Brick and other masonry materials, Building and Environment 15 (1981) 101–108.

[8] C. Hall, W.D. Hoff, M. Skeldon, The sorptivity of brick: dependence on the initial water content, Journal of Physics. D, Applied Physics 16 (10) (1983) 1875–1880.

[9] X. Qiu, F. Haghighat, M.K. Kumaran, Moisture transport across interfaces between autoclaved aerated concrete and mortar, Thermal Envelope and Building Science 26 (3) (2003) 213–236.

[10] A. Bouguerra, H. Sallée, F. de Barquin, R.M. Dheilly, M. Quéneudec, Isothermal moisture properties of wood-cementitious composites, Cement and Concrete Research 29 (1999) 339–347.

[11] P. Halamickova, R.J. Detwiler, D.P. Bentz, E.J. Garboczi, Water permeability and chloride ion diffussion in Portland cement mortars: relationship to sand content and critical pore diameter, Cement and Concrete Research 25 (4) (1995) 790–802.

[12] C. Hall, W.D. Hoff, Capillary rise in brick stacks, Ceramic Bulletin 71 (5) (1992) 767–769.

[13] D.C. Hughes, Pore structure and permeability of hardened cement paste, Magazine of Concrete Research 37 (133) (1985) 227–233.

[14] S. Tada, S. Nakano, Microstructural approach to properties of moist cellular concrete, in: F.H. Wittman (Ed.), Autoclaved Aerated Concrete, Moisture and Properties, Elsevier Scientific Publishing Company, Amtserdam, 1983, pp. 71–89.

[15] F.A.L. Dullien, Porous Media, Fluid Transport and Pore Structure, Academic Press, New York, 1979.

[16] M.S. Goual, A. Bali, M. Quéneudec, Effective thermal conductivity of clayey aerated concrete in the dry state: experimental results and modelling, Journal of Physics. D, Applied Physics 32 (1999) 3041–3046.

[17] B. Perrin, Etude des transferts couplés de chaleur et de masse dans les matériaux poreux consolidés non saturés utilisés en Génie Civil, Thèse de Doctorat d'état de l'Université Paul Sabatier, Toulouse (France), 1985.

[18] A. Hillerborg, A modified absorption theory, Cement and Concrete Research 15 (1985) 809–816.

[19] M. Douglas, Principles of Adsorption and Adsorption Processes, John Wiley & Sons, New York, 1984.

[20] Y. Couasnet, Contribution à l'étude du transfert de vapeur d'eau en régime permanent et non stationnaire dans les matériaux poreux hygroscopiques, Cahiers du CSTB, livraison 302, cahier 2349, in: C.S.T.B. (Centre Scientifique et Technique du Bâtiment) (Ed.), , 1989.

[21] J.R. Philip, D.A. De Vries, Moisture movement in porous material under temperature gradients, Transactions - American Geophysical Union 38 (2) (1957) 222–232.

[22] Autoclaved aerated concrete, properties, testing and design, in: S. Aroni, G.J. de Groot, M.J. Robinson, G. Svanholm, F.H. Wittman (Eds.), RILEM Technical Committers 78-MCA and 51-ALC, E & SPON, London, 1993.

[23] F.A.L. Dulien, Porous Media, Fluid Transport and Pore Structure, Academic Press, New York, 1979.

[24] F. Metz, D. Knöfel, Systematic mercury porosimetry investigations on sandstones, Materials and Structures 25 (1992) 127–136.

[25] J.M. Haynes, Determination of pore properties of constructional and other materials: general introduction and classification of methods, (RILEM), Materials and Structures 6 (33) (1973) 169–174.

[26] J. Van Keulen, Density of porous solid, (RILEM), Materials and Structures 6 (33) (1973) 181–183.

[27] Constant humidity with sulphuric acid solutions, in: R.C. Weast, S.M. Selby (Eds.), 48th Edition of the Handbook of Chemistry and Physics, The Chemical Rubber Co., Cleveland, Ohio, 1968, p. E36.

[28] R. Pigache, Etude et realisation d'un béton cellulaire autoclave à base de Loess, Thèse 3ème cycle, Géologie Appliquée, Universié de Lille-France, 1978, 199 pp.

[29] M. Ruzicka, Optimisation d'un procédé de moussage protéinique de pâtes argile-ciment: Conséquences sur le comportement physicomécanique du matériau durci, Thèsis de Doctorat, INSA de Lyon (France), 1998.

[30] Z.C. Moh, Reaction Accompanying Stabilization of Clay with Cement, Soil–Cement Stabilization: Highway Research Record Number 86, National Academy of Sciences, Washingthon, 1965.

[31] O.G. Ingles, J.B. Metclaf, Soil Stabilisation, Butter Worths (Eds), Melbourne, Australia, 1972, 189 pp.
[32] L.V. Goncharova, Processes of Cementation of Disperse Soils by Portland Cement, Trudy Soveshck, Po Teor. Osnovam Tekhn. Melior Gruntov, Moscow, 1960.
[33] J.M. Mitchel, S.A. El Jack, The fabric of soil–cement and its formation, in clays and clay minerals, Proceedings of the Fourteenth National Conference, Berkley, 1966.
[34] S. Brunauer, P.H. Emmet, E. Teller, Adsorption of gases in multimolecular layers, Journal of the American Chemical Society 60 (1938) 309.
[35] H.M. Künzel, Verfahren zur ein-und zweidimensionalen Berechnung des gekoppelten Wärme-un Feuchte transports in Bauteilen mit einfachen Kennwerten. Dissertation Universität Stuttgart (1994).
[36] C. Hall, T. Kam-Ming TSE, Water movement in porous building materials: VII. The Sorptivity of Mortars, Building and Environment 21 (2) (1986) 113–118.